ELECTRICAL BREAKDOWN IN WATER

Kulikov V.
PhD Dr Phys. Professor
Tomsk Agricultural Institute - a Branch of the Novosibirsk State Agrarian University, Tomsk, Russia
https://doi.org/10.5281/zenodo.10009518

Abstract
The process of formation of anodic electrical breakdown in the crystal structure of ice and liquid water is considered within the framework of the mechanism of generation of free charge carriers through interatomic Auger transitions in the valence band of the dielectric.

Keywords: mechanism of electrical breakdown in water, electrical strength of water

Introduction

Electrical breakdown in the form of a corona discharge is widely used for water disinfection [1]. The impulse electrical strength of liquid dielectrics turns out to be higher compared to solid ones. The construct with needle electrodes at the interface between the media ensures the introduction of a discharge into a solid dielectric. This effect allows the use of water in electric pulse technology for the destruction of rocks, concrete, and building materials [2-4]. The high dielectric permittivity and high pulse electrical strength of water (~ 0.5 MV/cm) make it possible to use water insulation in the forming line of pulsed high-current accelerators of charged particles in the megavolt range, which is an integrating RC circuit at the output of the pulse voltage generator. Water has another quality necessary for such systems - the ability to quickly restore electrical strength after a breakdown [5, 6].

The properties of electrical breakdown of ice and water are characteristic of solid and liquid dielectrics [7, 8]. According to work [6], the development of a discharge in water in a uniform field occurs from the positive electrode (anode breakdown). Optical imaging of the leader stage of breakdown showed that in an inhomogeneous electric field strength with ~10^5 V/cm, the average velocity of the positive leader (~$5 \cdot 10^6$ cm/s) significantly exceeded the average velocity of the negative leader (~$I0^5$ cm/s). As the leader moved deeper into the gap, his speed increased [6]. At a higher average field strength of ~10^6 V/cm with a point-plane electrode configuration, the velocity of the positive leader reached ~10^7 cm/s [9]. Measurements of the pre-breakdown conduction current using a bridge circuit with a positive polarity of the point electrode showed a current strength of ~ 0.3 A [10]. The electrical strength of ice (~0.3 MV/cm) is comparable to the strength of dielectrics such as PMMA (~0.37 MV/cm), PP (~0.4 MV/cm), glass (0.4 MV/cm) [2, 7].

The prospect of using water as insulation in electric pulse technologies and high-current accelerators of charged particles suggests the need for further study of the mechanism of electrical breakdown in water.

Previously, it was shown that anodic electrical breakdown in alkali halide crystals [11-18], quartz [19], semiconductor CdS [20], solid [21, 22] and liquid [23] organic substances with long chains of atoms is satisfactory is described by the mechanism of interatomic cascade Auger transitions. The appearance, movement and orientation of the electrical breakdown channel is determined taking into account data on the crystal chemical and energy structure of the substance.

In this work, the process of formation of an anodic channel of electrical breakdown in ice and liquid water is discussed within the framework of the mechanism of generation of free charge carriers through interatomic Auger transitions in the valence band of the dielectric.

Crystallographic and electronic structure of ice and water

Experimental and theoretical studies of the atomic and electronic structure of an isolated H_2O molecule, solid and liquid phases of water are quite numerous (for instance, [23-31]).

The structural features of hexagonal ice I_h have been studied quite well using X-ray diffraction and electron and neutron diffraction methods [23]. Calculation models of ordinary ice follow the Bernal-Fowler rules: each oxygen atom is at the center of a tetrahedron with four other oxygen atoms at its vertices, spaced 2.7 Å apart. Along all four nearest O-O directions there is an H atom, two of them form an O-H hydroxyl bond, the other two form an O···H hydrogen bond with the central O atom. Each water molecule is connected by hydrogen bonds to its four nearest neighbors: it gives off two hydrogen bonds and accepts two hydrogen bonds. This arrangement of molecules in a lattice produces significant intermolecular attraction. The lattice consists of layers perpendicular to the ***c*** axis of the crystal and containing hexagonal rings of water molecules. There are also hexagonal rings formed by three molecules in one layer and three molecules from the next layer (Fig. 1)

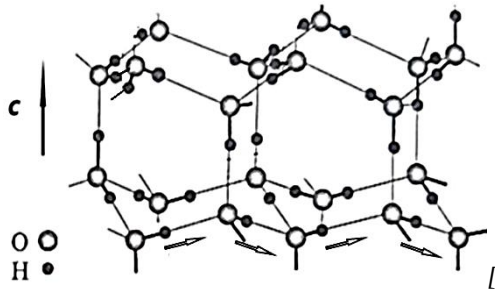

[23-27].

Fig. 1. System of intermolecular bonds in the hexagonal structure of ice [27]. The arrows show the movement of the breakdown channel

The sizes of water molecules in ice I_h differ slightly from the sizes of isolated molecules. For ice, the O-H distance is 1.01 Å (for an isolated water molecule 0.96 Å), and the H-O-H bond angle is probably slightly larger than the bond angle in an isolated molecule of 104.5 degrees [24].

The arrangement of protons is not easy to achieve experimentally, since spectroscopy methods mainly characterize the positions of oxygen atoms. The distribution of protons in the environment of the O atom must obey the Bernal-Fowler rules. However, there are many ways to distribute hydrogen atoms to realize such a global order. Variations in the O-H order in tetragonal coordination create dozens of ice phases [24, 25].

The authors of [24, 25], note that different ice structures are almost indistinguishable from the point of view of energy and local bond structure.

The energy eigenvalues of an isolated H_2O molecule arise as a result of interactions between the O 2s, O 2p and H 1s states of the atoms. The electronic structure of ice and water is constructed using water clusters [28, 29] or the solid state [30] using quantum chemical methods and Monte Carlo calculations. In the accepted notation [28-31], the eigenstates of a water molecule include 2a1 (O 2s with some H 1s character), $1b_2$ and $3a_1$ (O 2p hybridized with H 1s), $1b_1$ (non-bonding O 2p), and the lower unoccupied $4a_1$ (O 2s, 2p and H 1s) and $2b_2$ (O 2p and H 1s). States. $2a_1$, $1b_2$ and $3a_1$ belong to binding states, while $4a_1$ and $2b_2$ have anti-binding features (Fig. 2, a).

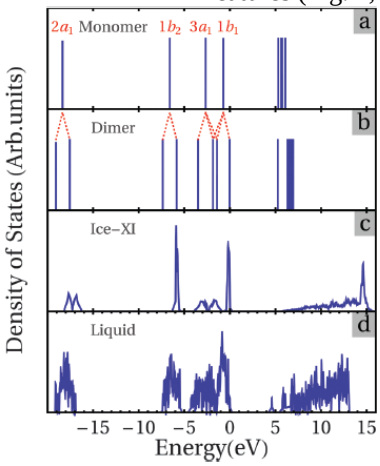

Fig. 2. Calculations of the intrinsic energies of isolated H_2O and its dimer, the density of states of the ice phase and water, simulated at 300 K [30]

For the dimer H_2O and Ice-XI the distortion of molecules and interactions between molecules cause splitting of the $1b_2$ states (about 1.5 eV) and further hybridization between the $3a_1$ and $1b_1$ states (Fig. 2, b, c). This gives a decrease in the new $3a_1$ states and an upward shift in the new $1b_1$, together with the creation of two new hybrid states (bonding $3a_1/1b_1$ and anti-bonding $(3a_1/1b_1)$* state) with two peaks around -3.2 eV and -1.6 eV, respectively. O 2p states dominate here, mixed with some H 1s character. The $1b_2$ band at -6 eV and the $1b_1$ band at the top of the valence band (set at 0 eV) show atomic orbital behavior with very small band widths. The lowest level $2a_1$ belongs to O 2s states hybridized with H 1s orbitals, with two peaks around -17.7 eV and -16.8 eV, respectively. The lower unoccupied $4a_1$ states also experience a decrease in energy due to further hybridization [30].

The split in the energies of the monomer orbitals during the formation of a dimer reflects the feature that each water molecule plays the role of a proton donor or acceptor. H - bonding involves mixing of $3a_1$ and $1b_1$ orbitals. This causes the $3a_1$ and $1b_1$ bands to expand during condensation [28, 29].

In the research [30], for Ice-XI the density of states (DOS) of the lower part of the conduction band (from about 5.6 to about +14.5 eV) is formed by O 2p/3s states mixed with some H 1s character. These states in the lower part of the conduction band show significant dispersion of more than 5 eV. The peak occurs at approximately 14.5 eV with a predominance of O 2p–H 1s states (anti-bonding, $4a_1$). The energy gap between the occupied and unoccupied states was 5.55 eV (Fig. 2, c, d).

According to calculations [30], the electronic structure of water at a temperature of 300 K is similar to the Ice-XI phase (Fig. 2, c, d). The DOS curves of water at 300 K are more dispersed; there are tails in localized states near the bottom of the conduction band. Opinion of the authors of [30], the obtained electronic structures and energy gaps for the ice and liquid water phases are in good agreement with the available experimental data.

Experimental studies of the band gap Wg of ice and water involve estimating the ionization potential obtained from measuring the photoelectron emission and electron affinity of water W_0 via inverse photoemission.

An analysis of the Wg values of ice and liquid water at ambient temperature, taking into account reliable recent experimental data, was made in [31]. The authors assume the ionization potential of liquid water to be ~10.0 eV. Electron affinity is estimated as W_0= -1.0 eV. The Wg value is ~9.0 eV. The hexagonal phase of ice is stable at ambient temperature and pressure and has been the subject of numerous experimental and theoretical studies. At a temperature of 77 K, the ionization potential is assumed to be ~10.3 eV, W_0 = -0.9 eV, which gives Wg = 9.4 eV.

Probably, a slight increase in the electron affinity of liquid water compared to W_0 ice is associated with the formation of defects or regions where free hydrogen atoms can interact with delocalized electrons [28, 29].

Obviously, there is no long-range ordering in liquid water. However, at short-range the structure of water is topologically the same as those of ice, but with flexible bond-lengths and angles of H_2O tetragons [30].

It can be concluded, that the electronic structures of the various phases of ice and liquid water are similar in shape and are in good agreement with the available experimental data.

Model of the electrical breakdown channel in water

The energy band diagram in the area of contact between the metal electrode and water in a strong electric field is shown in Fig. 3. The energy levels of the states of O and H atoms are given in accordance with the data from [30].

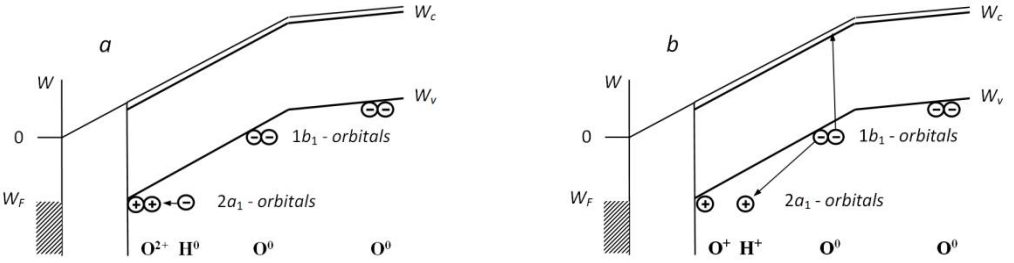

Fig. 3. Scheme of resonant (a) and Auger (b) transitions in water in a strong electric field. Wc, Wv, W_F - energy levels of the conduction band bottom, crystal valence band ceiling and the Fermi metal, respectively

According to [13-15], the beginning of the formation of a breakdown channel is determined by processes at the metal–insulator interface. At an average field strength in the sample of ~10^6 V/cm, the actual field strength near the microtips of the electrode can be more than ~10^8 V/cm [14]. In the near-electrode region of the dielectric, due to the tunneling transition of electrons into the metal, O^{2+} ions with two holes are formed in the $1b_1$ orbitals. For this, the required voltage *U* shall be such that the edge of the valence band of the dielectric will rise to the Fermi level of the metal. It is most likely that a neighboring hydrogen atom participates in the process of hole recombination through resonant electron transfer from the $3a_1$ level of hydrogen to the $1b_1$ level of oxygen. The process is realized with an energy increase in the $3a_1$ level by ~ 3 eV (Fig. 3, a). The decay of a hole into H^+ occurs as a result of the interatomic Auger transition of an electron from the $1b_1$ orbital of a neighboring O atom and the subsequent generation of an Auger electron into the conduction band (Fig. 3, b).

The transition of an Auger electron to the conduction band occurs provided that the minimum energy gap between the $3a_1$ orbitals of H^+ atoms and the $1b_1$ orbitals of O in the electric field is not less than the band gap of the dielectric. Issues related to estimating the electric field strength on the surface of the breakdown channel front are considered in [14, 15]. In alkali halides, the necessary band bends for Auger transitions are provided by the electric field of the space charge, which includes a layer of doubly and layers of singly charged halogen ions. The front of the breakdown channel coincides with the boundary of the space charge.

A single cycle of movement of the front of the fire can be divided into three successive stages. At the first stage, when the critical local electric field strength of 10^8 V/cm is reached, a resonant transition of the electron from H to the O^{2+} atom occurs in a time τ_r ~10^{-16} s and the channel moves to the interatomic distance (Fig. 3, a). The second stage is associated with the recombination of a hole on H^+ due to the interatomic Auger transition of an electron from a neighboring oxygen atom during a time τ_A ~10^{-16} s and the generation of an Auger electron into the conduction band of the dielectric. The channel moves one more interatomic distance (Fig. 3, b). The negative charge of electrons reduces the charge field of holes and, accordingly, the bending of bands near the boundary of the charge zone. The third stage is associated with the extraction of electrons by an external electric field from the space charge region, and the achievement of a critical field strength for the next cycle. Cycle time Δt can be represented as

$$\Delta t = \tau_r + \tau_A + \tau_1, \quad (1)$$

where τ_1 - time to reach the critical field strength.

The structure of the breakdown channel is formed by a set of single Auger transition channels (Fig. 1), passing in one direction, and includes a positive space

charge and a conducting channel of complex phase composition with electron-hole plasma.

The channel front moves from the positive electrode into the sample. The channel diameter is probably determined by the size of the area within which a layer of O^{2+} ions is formed in the near-surface region of the dielectric, and its size is proportional to the external voltage. This pattern was observed previously for KCl and KBr crystals, in which the diameter of the breakdown channel increased linearly with voltage in the range of 100−300 kV [8].

Conclusion

There is no long-range order in liquid water, but at short distances the crystallochemical structure of water is topologically the same as that of ice. The electronic structures of various phases of ice and liquid water are similar in shape and are in good agreement with the available experimental data. A model is proposed for the generation of free charge carriers in samples of crystalline ice and liquid water through interatomic Auger transitions in the valence band of the dielectric. The model satisfactorily interprets the anodic nature of the breakdown, high speeds of the breakdown channel of 10^7 cm/s, and prebreakdown current density ~ 10^4 A/cm^2.

References:

1. Kuzhekin I.P., Kurbanov E.D. Impul'snyy razryad v vode. Energetikanın problemleri. 2008. № 1. (in Russian)
2. Vorobyov G.A. Effect of Discharge Incorporation into a Solid Insulator Immersed in an Insulating Fluid. Tech. phys. 2005. V. 50. №4. p. 517.
3. Vazhov V.F., Koslova N.V. Impul'snaya elektricheskaya prochnost' vody i granita. Vestnik nauki Sibiri. 2012. № 1 (2) .s. 79. (in Russian)
4. Petrov Yu. V., Morozov V. A., Smirnov I. V. and Lukin A. A. Electrical Breakdown of a Dielectric on the Voltage Pulse Trailing Edge: Investigation in Terms of the Incubation Time Concept. Tech. phys. 2015. V.60. № 12. pp. 1733-1737. DOI: 10.1134/S1063784215120178
5. Arbuzov A. I., Bystritskiy V. I., Krasik Ya. E, Lopatin V. S., Usov Yu. P., Tolmacheva V. G., Chistyakov S. A. Sil'notochnyy uskoritel' s vodyanym nakopitelem. Trudy 6 vsesoyuznogo soveshchaniya po uskoritelyam zaryazhennykh chastits. Dubna. 1978. 11-13 oktyabrya. s. 75. (in Russian)
6. Vorobyov V. V. Mekhanizm proboya vodyanogo dielektrika sil'notochnykh impul'sivnykh uskoriteley zaryazhennykh chastits (Dis. kand. fiz.-mat. nauk. Novosibirsk, 1984). (in Russian)
7. Vorobyov A.A., Vorobyov G.A. Electricheskiy proboi i razrushenie tverdykh tel (Izda-vo Vysshaya shkola, M., 1966), 224 s. (in Russian)
8. 8. Vershinin Yu. N. Elektronno-teplovye i detonatsionnye protsessy pri elektricheskom proboe tverdykh dielektrikov (Izda-vo UrO RAN, Ekaterinburg, 2000), 260 s. (in Russian)
9. Punanov I.F. Prostranstvenno-vremennye i energeticheskie kharakteristiki vysokovoltnogo nanosekundnogo proboya kondensirovannykh dielektrikov (Dis. kand.fiz.-mat.nauk. (Yekaterinburg, UrFU, 2017). (in Russian)
10. Ovchinnikov I.T., Yanshin E.V. Izmereniye predproboynoy elektroprovodnosti vody s pomoshch'yu impul'snogo vysokovol'tnogo elektroopticheskogo mosta. V kn. Impul'snyy razryad v dielektrikakh. (Izda-vo Nauka, Novosibirsk, 1985), s. 83-88. (in Russian)
11. Kulikov V. D. The mechanism of the streamer stage of breakdown in crystal dielectrics. Tech. Phys. Lett. 2000. V. 26. № 2. pp. 170-172. DOI: 10.1134/1.1262781
12. Kulikov V. D. Charge Carrier Generation in a KBr Crystal under the Action of a Pulsed Sub-Breakdown Electric Field. Tech. Phys. Lett . 2002. V. 28. № 2. pp. 99-101. DOI: 10.1134/1.1458502
13. Kulikov V. D. Electrical Breakdown in Ionic Crystals Exposed to Nanosecond Pulses. Tech. Phys. 2003. V. 48. № 12. pp. 1527-1531. DOI: 10.1134/1.1634672
14. Kulikov V. D. Electrical Breakdown in Ionic Crystals. Tech. Phys. 2009. V. 54. № 1. pp. 56-61. DOI:10.1134/S1063784209010083
15. Kulikov V. D. Model of the Electrical Breakdown Channel in Ionic Crystals. Tech. Phys. 2012. V. 57. № 2. pp. 192-197. DOI:10.1134/S1063784212020144
16. Emlin R. V., Barakhvostov S. V., Kulikov V. D. Anisotropy of Electrical Breakdown in Crystalline Quartz. Tech. Phys. 2009. V. 54. № 7. pp. 1076-1079. DOI:10.1134/S1063784209070275
17. Kulikov V. D. Electrical Breakdown in Ionic Crystals (Izda-vo Tomsk St. Univ. Tomsk, 2014). (in Russian)
18. Punanov I.F., Emlin R. V., Kulikov V. D. and Cholakh S.O. Resistance of a Pulsed Electrical Breakdown Channel in Ionic Crystals. Tech. Phys. 2014. V.59. № 4. pp. 503-507. DOI: 10.1134/S1063784214040197
19. Kulikov V., Yakovlev V., Bobkova L. Model of a streamer discharge channel in monocrystalline CdS. NJDIS. 2020. № 44-1. pp. 21-24.
20. Kulikov V. Electrical breakdown of polymeric materials. NJDIS.№ 62-1. pp. 51-54. 2021. DOI:10.24412/3453-9875-2021-62-1-51-54
21. Kulikov V. Barrier effect in dielectric materials. NJDIS. 2023. № 62-1.pp. 51-54. DOI: org/10.5281/zenodo.7688048
22. Emlin R.V., Punanov I.F., Kulikov V.D. Electronic mechanism of propagation of nanosecond breakdown channel in liquid organic dielectrics. Tech. Phys. 2022. V. 92. № 10. pp. 1342-1348. DOI: 10.21883/TP.2022.10.54361.93-22
23. Zatsepina G. N. Fizicheskiye svoystva i struktura vody. (Izda-vo Moskov St. Univ, Moskva, 1998). 184 s. (in Russian)
24. Eisenberg D. S., Kauzmann W. The structure and properties of water (Oxford University Press, N.Y., 1969). 296 p.
25. Casassa S., Calatayud M., Doll K., Minot C. and Pisani C. Proton ordered cubic and hexagonal periodic models of ordinary ice. Chem. Phys. Lett. 2005. **409**. 110. DOI: org/10.1016/j.cplett.2005.04.068

26. Macher M., Klimeˇs J., Franchini C., and Kresse G. The random phase approximation applied to ice. J. Chem. Phys. 2014. **140**. 084502.

27. Tret'yakov Yu. D. Neorganicheskaya khimiya (Izda-vo ACADEMA, Moskva, 2004). T. 2. 366 s. (in Russian)

28. P. Cabral do Couto, S. G. Estácio, and B. J. Costa Cabrala. The Kohn-Sham density of states and band gap of water: From small clusters to liquid water. J. Chem. Phys. 2005. **123**, 054510 . DOI: 10.1063/1.1979487

29. P. Cabral do Couto, B. J. Costa Cabral, S. Canuto. Electron binding energies of water clusters: Implications forthe electronic properties of liquid water. Chem. Phys. Lett. 2006. **429.** pp. 129–135. DOI: 10.1016/j.cplett.2006.08.046

30. Changming Fang, Wun-Fan Li, Rik S. Koster, Jiri Klimes, Alfons van Blaaderen and Marijn A. van Huisa. The accurate calculation of the band gap of liquidwater by means of GW corrections applied toplane-wave density functional theory molecular dynamics simulations. Phys. Chem. Chem. Phys. 2015. **17.** p. 365. DOI: 10.1039/c4cp04202f

31. Bischoff T., Reshetnyak I. and Pasquarello A. Band gaps of liquid water and hexagonal ice through advanced electronic-structure calculations. Phys. Rev. Research, 2021. **3.** 023182 . DOI: 10.1103/PhysRevResearch.3.023182